

Doppler Signature Analysis of Mixed O/X-Mode Signals in Over-The-Horizon Radar

Ammar Ahmed and Yimin D. Zhang
Department of Electrical and Computer Engineering
College of Engineering, Temple University
Philadelphia, PA 19122, USA

Braham Himed
RF Technology Branch
Air Force Research Lab (AFRL/RYMD)
WPAFB, OH 45433, USA

Abstract—We analyze the Doppler signatures of local multipath signals in an over-the-horizon radar in the presence of both ordinary (O) and extraordinary (X) polarization modes. As the ionospheric signal reflection for the two polarization modes varies from each other, the existing local multipath model developed for a single polarization mode must be extended to account for such a propagation environment. In this paper, we focus on the case with small delays between the signals corresponding to the two propagation modes. We exploit the multipath signal model considering the mixed O/X mode signals and analyze the variation in the resulting Doppler signatures. The analytical as well as numerical results show that the existence of both O/X polarization modes renders more signal components with close Doppler signatures. In the underlying situation with small delays between the two modes, the mixed O/X-mode signals corresponding to each local multipath signal component are unresolvable and yield time-varying fading magnitude. Accurate parameter estimation is still achieved using fractional Fourier transform over a longer coherent processing time.

Keywords: Doppler parameter estimation, fractional Fourier transform, over-the-horizon radar, target localization, time-frequency analysis.

I. INTRODUCTION

Sky-wave over-the-horizon radar (OTHR) is designed to provide long-range surveillance capability of targets that are far beyond the limit of the Earth horizon [1–6]. Significant research efforts have been invested to estimate the target parameters in OTHR systems [7–13]. One of the most important parameters that enables target classification is target altitude. However, direct estimation of the target altitude is often difficult because of the narrow-band nature of the OTHR signals and the uncertain ionospheric conditions. Generally, existing target altitude estimation strategies for OTHR [14–24] can be classified into three main categories: (a) target tracking with the target altitude being considered as one of the target state parameters [8, 10–12, 22, 23], (b) joint ionosphere and target parameter estimation based on their statistical models [13, 21], and (c) local multipath signal characterization using high-resolution time-frequency analysis [14–19, 24].

The local multipath model developed in [8] is considered effective for target altitude estimation [17–20]. In this model, the round-trip OTHR signals directly reflected by the ionosphere layer and that is also reflected by the specular ground/ocean surface generate three spectrally equidistant

Doppler components. The average Doppler component and the Doppler separation helps in estimating the target parameters, such as the vertical velocity and altitude [18].

In practice, due to the Earth’s magnetic field, two propagation modes exist in the ionosphere corresponding to different polarizations of the electromagnetic wave, termed as ordinary (O) and extraordinary (X) polarization modes [25, 26]. Signals associated with these two polarization modes are reflected at their respective heights in the ionosphere, thereby resulting in distinct slant ranges for each mode. When these paths differ significantly in their reflection heights, high-precision ionograms enable separation of these two polarization modes [27]. On the other hand, their separation is challenging when the difference between their reflection heights is small. In this case, the existing signal model and target parameter estimation and tracking techniques developed for OTHR under the single-mode propagation model must be re-examined.

In this paper, we analyze the Doppler signatures of the OTHR signals under a local multipath signal model, considering both O/X polarization modes with a small difference in their reflection heights. The resulting Doppler signatures obtained from the mixed O- and X-mode multipath model are investigated and compared to those obtained from the conventional single-mode multipath propagation model. Our analysis reveals that additional Doppler components are introduced as the result of the two modes when compared with the conventional single-mode multipath propagation case. The mixed O/X-mode signals corresponding to each local multipath are unresolvable and appear as a single component in the time-frequency domain whose instantaneous Doppler frequency becomes a weighted average of the two closely spaced individual average Doppler components corresponding to the two modes. The Doppler signatures corresponding to different local multipath components remain separable through high-resolution time-frequency analysis when a sufficiently long coherent processing interval (CPI) is considered. The Doppler characteristics of the X-mode signal is similar to those of the O-mode signal except for a small frequency shift that is shared for all the local multipath components. Simulation results are presented to confirm this mathematical analysis.

II. LOCAL MULTIPATH SIGNAL MODEL FOR MIXED O/X-MODE SIGNALS

Generally, O- and X-mode signals are reflected by the ionosphere at different heights, which are often referred to as the virtual ionosphere heights, depending on the operating frequency and the incidence angle [25–27]. We consider a

The work of A. Ahmed and Y. D. Zhang is supported in part by a sub-contract with Matrix Research, Inc. for research sponsored by the Air Force Research Laboratory under Contract FA8650-14-D-1722.

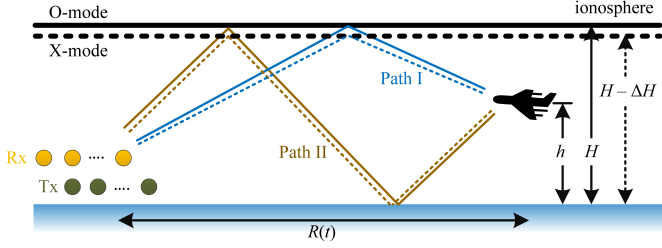


Fig. 1. Flat-Earth local multipath propagation model of OTHR for O-mode (solid lines) and X-mode (dashed lines) polarized waves. The two heights of the ionosphere illustrate the virtual ionosphere heights for the respective modes.

simplified flat-earth multipath signal model as illustrated in Fig. 1, where the two modes correspond to different virtual ionosphere heights for the O- and X-mode signals. Without loss of generality, we consider the case where the virtual ionosphere height for the X-mode wave is lower than that of the O-mode wave; however, the same analysis remains valid if the converse is true. We denote H as the virtual ionosphere height for the O-mode wave, $H - \Delta H$ as the virtual ionosphere height for the X-mode wave assuming $0 < \Delta H \ll H$, and h as the target altitude. We assume that a *coarse* estimate of the ionosphere height is known from the ionosonde monitoring. Moreover, stable ionospheric conditions are considered such that the height of the ionosphere does not vary during the CPI. For mathematical convenience, we also assume that the O- and X-mode signals share the same operational frequency.

As shown in Fig. 1, the two polarization modes render different round-trip propagation paths, respectively depicted by solid and dashed lines. For each polarization mode, each of the forward and return paths can take path I (directly reflected by the ionosphere) or path II (reflected by the ionosphere and the Earth surface). As a result, for each mode, the signals received at the OTHR receiver follow the following three distinct round-trip paths: (a) Round-trip path 1: emitted and received along path I; (b) Round-trip path 2: emitted and received along path II; and (c) Round-trip path 3: emitted along path I and received along path II, and vice versa. In the following, we first consider the slant range and Doppler signatures for the O-mode wave, and the results are extended to the X-mode wave.

In Fig. 2, we illustrate an equivalent local multipath model for the O-mode wave to simplify the analysis of slant range computations [14, 18]. A similar figure can also be constructed for the X-mode wave signals. The target and the propagation paths below the ionosphere are the true ones, whereas those above the ionosphere are their mirrored version due to reflections in the ionosphere and the Earth surface. The one-way slant ranges of path I and II, respectively denoted as $l_{o,1}$ and $l_{o,2}$, can be expressed in terms of the ground range R , the respective virtual ionosphere height H , and the target altitude h , as:

$$l_{o,1} = (R^2 + (2H - h)^2)^{0.5}, \quad (1a)$$

$$l_{o,2} = (R^2 + (2H + h)^2)^{0.5}. \quad (1b)$$

In this paper, we consider the situation that a target flies with a fixed altitude and a constant horizontal velocity. As such, $l_{o,1}$, $l_{o,2}$, and R are time-varying, whereas H and h remain constant. We omit the explicit notation of (t) throughout

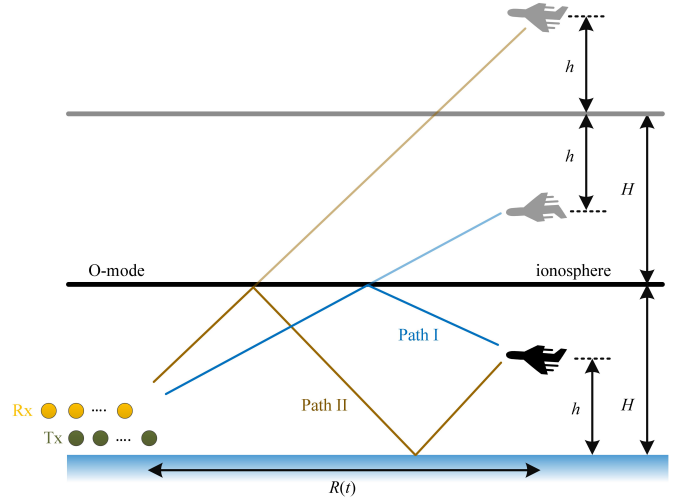


Fig. 2. Equivalent local multipath propagation model for the O-mode wave.

this paper for notational simplicity. Assuming $h \ll H \ll R$, and using Taylor approximation, we obtain the following simplified one-way slant range equations:

$$l_{o,1} \approx R + \frac{2H^2 - 2Hh}{R}, \quad (2a)$$

$$l_{o,2} \approx R + \frac{2H^2 + 2Hh}{R}. \quad (2b)$$

The slant range of the three round-trip paths for the O-mode wave can be respectively expressed as:

$$L_{o,1} = 2l_{o,1}, \quad L_{o,2} = 2l_{o,2}, \quad L_{o,3} = l_{o,1} + l_{o,2}. \quad (3)$$

Similar slant range formulations can also be developed for the X-mode wave signals by replacing H by $H - \Delta H$ in Eq. (2). In this paper, we only consider the scenario where the difference in virtual heights corresponding to the two polarization modes is small such that $\Delta H \ll h \ll H$ is satisfied.

III. DOPPLER SIGNATURE ANALYSIS

The two-way slant ranges for the O-mode wave can be used to determine the corresponding Doppler signatures as:

$$f_{o,i} = -\frac{f_c}{c} \frac{dL_{o,i}}{dt}, \quad i = 1, 2, 3, \quad (4)$$

where f_c denotes the carrier frequency, c is the velocity of the electromagnetic wave, and i denotes the path index. For this case, we can obtain:

$$\frac{dl_{o,1}}{dt} \approx \dot{R} - 2\frac{H\dot{R}}{R^2}(H - h), \quad (5a)$$

$$\frac{dl_{o,2}}{dt} \approx \dot{R} - 2\frac{H\dot{R}}{R^2}(H + h), \quad (5b)$$

where $\dot{R} = dR/dt$. Note that a positive value of the target velocity \dot{R} is defined for the target moving away from the radar. The Doppler frequencies of the three different paths for the O-mode wave in Eq. (4) take the following simplified form:

$$f_{o,1} = \bar{f}_o + \Delta f_o, \quad (6a)$$

$$f_{o,2} = \bar{f}_o - \Delta f_o, \quad (6b)$$

$$f_{o,3} = \bar{f}_o. \quad (6c)$$

where

$$\bar{f}_o = -\frac{f_c}{c} \frac{d(l_{o,1} + l_{o,2})}{dt} \approx -\frac{2f_c}{c} \dot{R} + \frac{4f_c H^2 \dot{R}}{cR^2}, \quad (7a)$$

$$\Delta f_o = -\frac{f_c}{c} \frac{d(l_{o,1} - l_{o,2})}{dt} \approx -\frac{4f_c H h \dot{R}}{cR^2}. \quad (7b)$$

From Eqs. (6) and (7), we observe that the Doppler signatures of the round-trip paths 1 and 2 are symmetric around the round-trip path 3. The average Doppler component, \bar{f}_o , is shared by all three paths, and Δf_o denotes the frequency difference between the Doppler components corresponding to different local multipath signal components. Note that both \bar{f}_o and Δf_o are proportional to \dot{R} .

We can make similar observations for the Doppler components associated with the X-mode wave. The Doppler frequencies of the three different paths for the X-mode signals are expressed as:

$$f_{x,1} = \bar{f}_x + \Delta f_x, \quad (8a)$$

$$f_{x,2} = \bar{f}_x - \Delta f_x, \quad (8b)$$

$$f_{x,3} = \bar{f}_x, \quad (8c)$$

where \bar{f}_x and Δf_x are obtained by replacing H by $H - \Delta H$ in Eq. (7), expressed as:

$$\begin{aligned} \bar{f}_x &\approx -\frac{2f_c}{c} \dot{R} + \frac{4f_c(H - \Delta H)^2 \dot{R}}{cR^2} \\ &= \bar{f}_o - \frac{4f_c \dot{R}}{cR^2} (2H\Delta H - \Delta H^2), \\ \Delta f_x &\approx -\frac{4f_c(H - \Delta H)h\dot{R}}{cR^2} \\ &= \Delta f_o + 4\frac{f_c h \dot{R}}{cR^2} \Delta H. \end{aligned}$$

As $\Delta H \ll h \ll H \ll R$, we can simplify the above equations as:

$$\bar{f}_x \approx \bar{f}_o - 8\frac{f_c H \Delta H \dot{R}}{cR^2} = \bar{f}_o - f_\delta, \quad (9a)$$

$$\Delta f_x \approx \Delta f_o. \quad (9b)$$

Therefore, it becomes clear that the Doppler differences between the local multipath signal components are approximately the same for both O- and X-modes. Moreover, the average Doppler frequencies of both modes differ in magnitude only by $f_\delta = 8f_c H \Delta H \dot{R} / (cR^2)$. From Eqs. (7b) and (9a), we have:

$$f_\delta = 2\frac{\Delta H}{h} \Delta f_o. \quad (10)$$

Therefore, for the underlying scenario when $\Delta H \ll h$ holds, $f_\delta \ll \Delta f_o \ll \bar{f}_o$ remains valid. Further, from Eqs. (6)–(9), we observe that f_δ is shared for all local multipath pairs, i.e.,

$$f_\delta = f_{o,i} - f_{x,i}, \quad i = 1, 2, 3. \quad (11)$$

This implies that the three Doppler components respectively generated by O- and X-mode waves are displaced in the spectral domain by a small and common frequency shift f_δ .

We express the overall noise-free signal at the OTHR receiver as:

$$y(t) = \sum_{i=1}^3 \left(A_{o,i} e^{j(2\pi \int_0^T f_{o,i} dt + \phi_{o,i})} + A_{x,i} e^{j(2\pi \int_0^T f_{x,i} dt + \phi_{x,i})} \right), \quad (12)$$

where $A_{o,i}$ and $A_{x,i}$ denote the respective signal magnitudes for the O- and X-mode wave paths, and $\phi_{o,i}$ and $\phi_{x,i}$ are the corresponding initial phases. Since $f_{o,i}$ and $f_{x,i}$ have very close spectral proximity, the two components are unresolvable and thus are merged together, yielding three resolvable Doppler components expressed in the following form:

$$y(t) \approx \sum_{i=1}^3 W_i e^{j(2\pi \int_0^T (\zeta f_{o,i} + (1-\zeta) f_{x,i}) dt + \phi_i)}. \quad (13)$$

Here, $0 \leq \zeta \leq 1$, and the exact value of ζ and that of the overall phase term ϕ_i depend on the relative magnitude and phase relationship of the two modes. Moreover, W_i is a beating fading function whose frequency is associated with f_δ .

The Doppler frequencies of the three resolvable Doppler components are respectively centered at:

$$f_{ox,i} = \zeta f_{o,i} + (1 - \zeta) f_{x,i}, \quad (14)$$

for $i = 1, 2, 3$. The maximum possible frequency deviation between the resulting Doppler components in Eq. (13) with the corresponding individual O- and X-mode frequency signatures will be f_δ . For a special case where $A_{o,i} = A_{x,i} = A$ for all values of i , we obtain $\zeta = 0.5$, i.e., $f_{ox,i} = (f_{o,i} + f_{x,i})/2$, and the corresponding maximum frequency deviation becomes $f_\delta/2$.

IV. DOPPLER SIGNATURE ESTIMATION

For the underlying scenario where the target has a fixed altitude and moves with a constant horizontal velocity, the signal $y(t)$ in Eq. (12) consists of the sum of three parallel chirp signals which can also be observed from Fig. 3. Therefore, the fractional Fourier transform (FrFT) is effective to separately analyze the individual Doppler signatures. The α -angle FrFT of signal $y(t)$, denoted as $\mathcal{Y}_\alpha(z)$, is defined as [28, 29]:

$$\mathcal{Y}_\alpha(z) = \int_{-\infty}^{\infty} y(t) \mathcal{K}_\alpha(t, z) dt, \quad (15)$$

where z is the angular fractional frequency, and $\mathcal{K}_\alpha(t, z)$ is the kernel, given by:

$$\mathcal{K}_\alpha(t, z) = \begin{cases} \sqrt{\frac{1 - j \cot(\psi)}{2\pi}} e^{j \frac{z^2}{2} \cot(\psi)} \\ \quad \times e^{j \frac{t^2}{2} \cot(\psi)} e^{-j z \csc(\psi)}, & \psi \neq k\pi, \\ \delta(t - z), & \psi = 2k\pi, \\ \delta(t + z), & \psi + \pi = 2k\pi, \end{cases}$$

k is a non-negative integer, and $\psi = \alpha\pi/2$. Once the optimal rotation angle α_{opt} for each of the three chirps is determined

TABLE I. KEY PARAMETERS (UNLESS OTHERWISE SPECIFIED)

Parameter	Notation	Value
Initial range	$R(0)$	2,500 km
O-mode ionosphere height	H	350 km
X-mode ionosphere height	$H - \Delta H$	349 km
Target altitude	h	20 km
Target horizontal velocity	v_R	500 m/s
Carrier frequency	f_c	16 MHz
Pulse repetition frequency	f_s	140 Hz
Coherent integration time	T	120 s

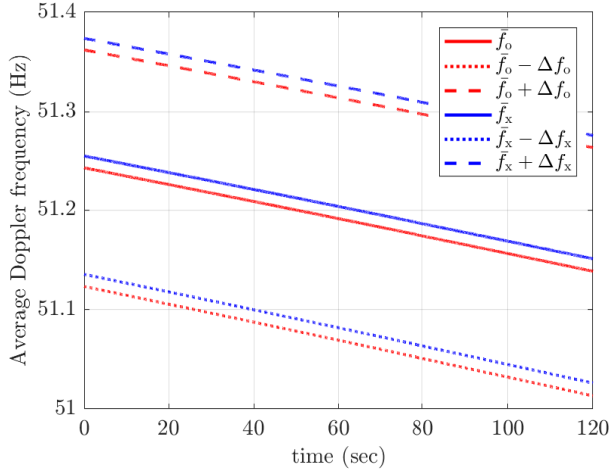


Fig. 3. The resulting Doppler components for both O mode (red color) and X mode (blue color).

through peak detection, we find the corresponding chirp rate $\hat{\gamma}$ as [28, 29]:

$$\hat{\gamma} = -\cot\left(\alpha_{\text{opt}} \frac{\pi}{2}\right) \frac{f_s^2}{N}, \quad (16)$$

where f_s is the pulse repetition frequency, and N is the number of samples used for calculating the FrFT. The centroid frequency of the chirp can be estimated as [30]:

$$f_{\text{centroid}} = \frac{f_{\text{frft}}}{\sin(\alpha_{\text{opt}} \pi/2)}, \quad (17)$$

where $f_{\text{frft}} = z_{\text{peak}} f_s / \pi$ and z_{peak} denotes the estimated peak angular frequency of the individual chirp in the fractional domain.

Performing FrFT over the linear Doppler signatures in the time-frequency domain accumulates the signal energy over the entire CPI. For the underlying mixed O/X-mode signals, it also effectively mitigates the effect of multi-mode fading so as to achieve robust parameter estimation.

V. SIMULATION RESULTS

In this section, we numerically examine the Doppler frequency components generated from the O- and X-mode waves, and compare them with the results obtained from the single-mode multipath model counterpart. The default parameters for the simulations are listed in Table I.

Fig. 3 shows the three Doppler components for each of the O- and X-modes based on Eq. (4), yielding a total number of six components. It is confirmed that the difference Doppler component due to local multipath is the same for both modes, i.e., $\Delta f_o = \Delta f_x$. Moreover, the frequency difference between the corresponding O-mode and X-mode signals, represented by $f_{o,i} - f_{x,i}$, remains a constant for the three Doppler components, thus confirming Eq. (11).

Next, we evaluate the spectrogram for the received local multipath signals, respectively for the mixed O/X-mode case and the O-mode only case. The same propagation attenuation is assumed for both polarization modes and all local multipaths.

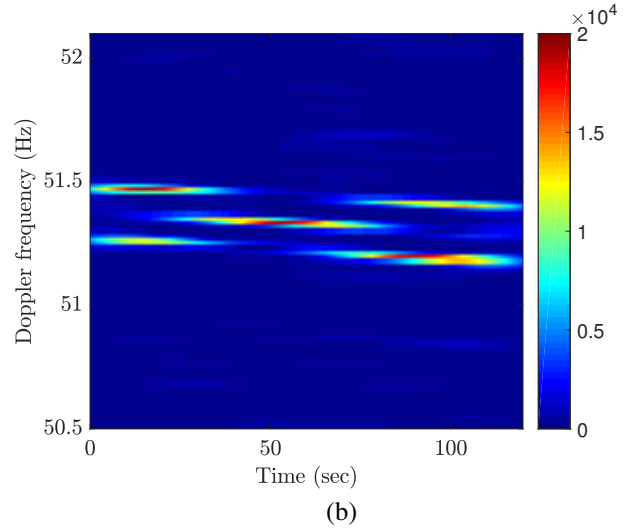
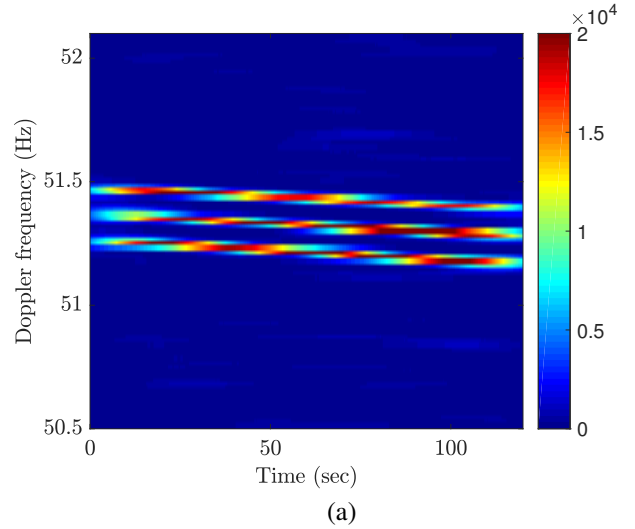


Fig. 4. Spectrogram of the received OTHR signals using a Hamming window of size 4096: (a) O-mode signal, (b) mixed O/X-mode signals.

For each case, independent zero mean white complex Gaussian noise is added to yield a signal-to-noise ratio (SNR) of -15 dB. Figs. 4(a) and 4(b) respectively show the spectrograms of the resulting O-mode signal and the mixed O/X-mode signal. For the single-mode case depicted in Fig. 4(a), each of the three local multipath Doppler components has a stable magnitude with respect to time. For the mixed O/X-mode signals depicted in 4(b), we confirmed that the six components are merged into three separable signatures, and their magnitudes vary with time as a beating fading, as discussed in Section IV.

Figs. 5(a) and 5(b) show the FrFT results of the O-mode signal and the mixed O/X-mode signal, respectively. For O-mode signals, we detect the three peaks, which appear at a rotation angle $\alpha = 0.9995$ in Fig. 5(a). For the mixed O/X-mode signal depicted in Fig. 5(b), the three chirp signals are also clearly detected with slightly lower magnitudes as a result of fading between the two polarization modes.

Fig. 6 shows the parameter estimation results corresponding to Fig. 5. Since all the signals share the same chirp rate, we first compute the optimal rotation angle α_{opt} by searching

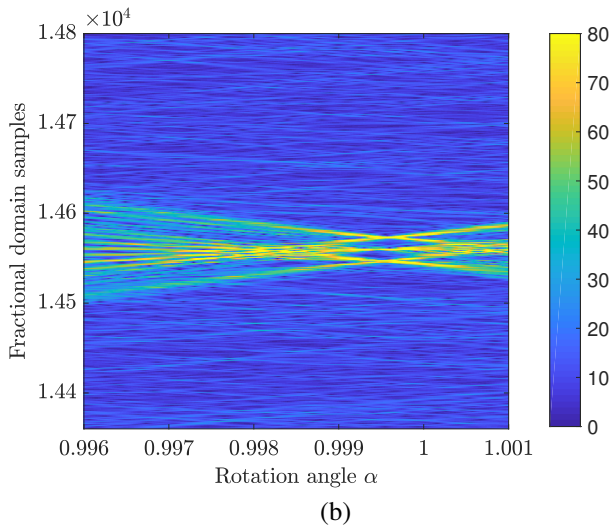
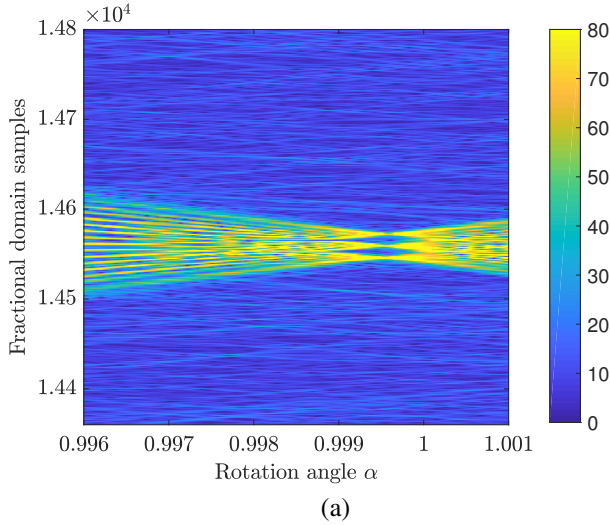


Fig. 5. FrFT of the received OTHR signals: (a) O-mode signal, (b) mixed O/X-mode signal.

the maximum magnitude of the FrFT with respect to α in Fig. 5. After α_{opt} is determined, we estimate the fractional frequencies by keeping $\alpha = \alpha_{\text{opt}}$ and exploiting the peak detection in the fractional frequency domain. The resulting peak fractional frequencies are fed in Eq. (17) to estimate the centroid frequencies of three chirps. It can be observed in Fig. 6 that the chirp rate and the fractional frequencies are clearly detected for both the O-mode signal and the mixed O/X-mode signal. However, the mixed O/X-mode signal yields lower peaks and reduced concentration due to the fading.

Based on Fig. 3, we obtain the theoretical value of the centroid frequencies corresponding to the three local multipath Doppler components for the O-mode signal to be 51.07 Hz, 51.19 Hz, and 51.31 Hz, respectively, whereas the respective Doppler frequencies for the mixed O/X-mode signal are 51.08 Hz, 51.20 Hz, and 51.32 Hz. From Fig. 6(a), the centroid frequencies of the estimated three local multipath Doppler components for the O-mode signal are obtained as 51.20 Hz, 51.31 Hz, and 51.42 Hz, respectively, whereas those obtained from Fig. 6(b) for the mixed O/X mode signal are respectively 51.21 Hz, 51.31 Hz, and 51.43 Hz. In both cases, the estimated

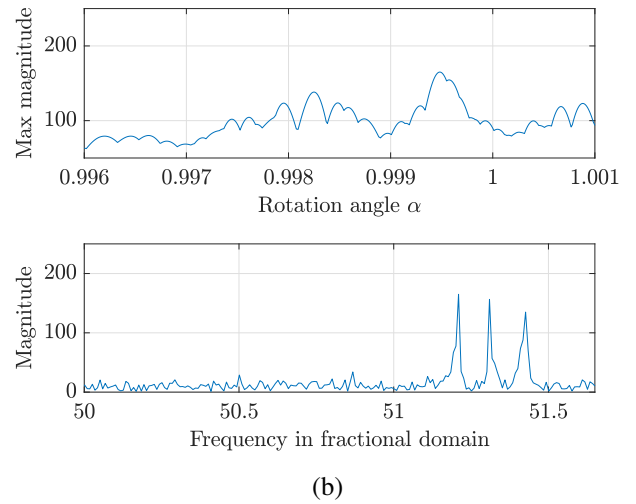
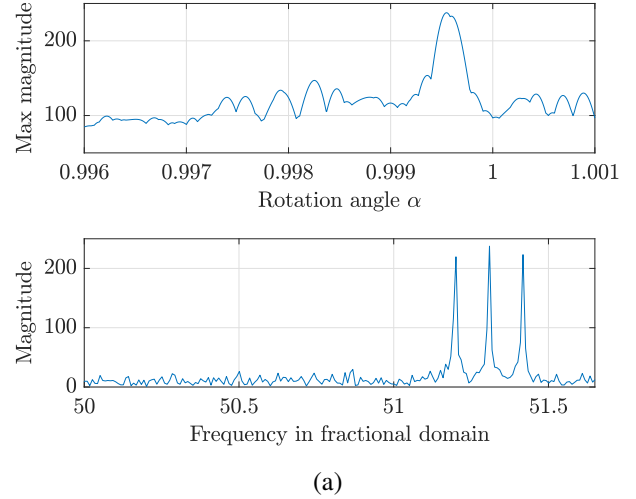


Fig. 6. FrFT parameter estimation: (a) O-mode signal, (b) mixed O/X-mode signal.

results have a good agreement with the theoretical values, demonstrating the effectiveness of the FrFT-based approach for parameter estimation in the presence of mixed O/X-mode signals with closely separated virtual heights.

VI. CONCLUSION

In this paper, we have investigated the OTHR signals for the case with mixed O/X-mode polarizations which exhibit a small difference in their virtual ionospheric heights. We observe that the mixed O/X-mode signals provide similar results compared to the case when the single-mode wave propagation is considered. Due to the small difference in the yielding slant ranges and Doppler signatures, the resulting signals corresponding to the two modes are not resolvable. As such, the overall signals render three local multipath signal components with each component being faded as a result of merging the signals corresponding to the two polarization modes together. As a result, the FrFT-based processing developed for a single-mode case can still be applied to obtain the Doppler parameters of the local multipath signal components.

VII. REFERENCES

- [1] M. Headrick and M. I. Skolnik, "Over-the-horizon radar in the HF band," *Proc. IEEE*, vol. 62, no. 6, pp. 664–673, June 1974.
- [2] A. A. Kolosov, *Over-the-Horizon Radar*. Artech House, 1987.
- [3] G. J. Frazer, Y. Abramovich, B. A. Johnson, "Use of adaptive non-causal transmit beamforming in OTHR: Experimental results," in *Proc. Int. Conf. Radar*, Adelaide, Australia, Sept. 2008, pp. 311–316.
- [4] J. M. Headrick and S. J. Anderson, "HF over-the-horizon radar," Chapter 20 in M. Skolnik (ed.), *Radar Handbook, 3rd Ed.* McGraw-Hill, 2008.
- [5] G. A. Fabrizio, *High Frequency Over-the-Horizon Radar: Fundamental Principles, Signal Processing, and Practical Applications*. McGraw-Hill, 2013.
- [6] G. J. Frazer, "Experimental results for MIMO methods applied in over-the-horizon radar," *IEEE Aerosp. Electron. Syst. Mag.*, vol. 32, no. 12, pp. 52–69, Dec. 2017.
- [7] W. Wang, Y. Peng, T. Quan, and Y. Liu, "HF OTHR target detection and estimation subsystem," *IEEE Aerosp. Electron. Syst. Mag.*, vol. 14, no. 4, pp. 39–45, April 1999.
- [8] R. H. Anderson, S. Kraut, and J. L. Krolik, "Robust altitude estimation for over-the-horizon radar using a state-space multipath fading model," *IEEE Trans. Aerospace Electron. Syst.*, vol. 39, no. 1, pp. 192–201, Mar. 2003.
- [9] K. Lu, and X. Liu, "Enhanced visibility of maneuvering targets for high-frequency over-the-horizon radar," *IEEE Trans. Antennas Propag.*, vol. 53, no. 1, pp. 404–411, Jan. 2005.
- [10] D. Bourgeois, C. Morisseau, and M. Flecheux, "Over-the-horizon radar target tracking using multi-quasi-parabolic ionospheric modelling," *IEE Proceedings - Radar, Sonar and Navig.*, vol. 153, no. 5, pp. 409–416, Oct. 2006.
- [11] K. Bell, "MAP-PF multi-mode tracking for over-the-horizon radar," in *Proc. IEEE Radar Conf.*, Atlanta, GA, May 2012, pp. 326–331.
- [12] H. Lan, Y. Liang, Q. Pan, F. Yang, and C. Guan, "An EM algorithm for multipath state estimation in OTHR target tracking," *IEEE Trans. Signal Process.*, vol. 62, no. 11, pp. 2814–2826, June 2014.
- [13] J. Hu, M. Li, Q. He, Z. He, and R. S. Blum, "Joint estimation of MIMO-OTH radar measurements and ionospheric parameters," *IEEE Trans. Aerospace Electron. Syst.*, vol. 53, no. 6, pp. 2789–2805, June 2017.
- [14] Y. D. Zhang, M. G. Amin, and G. J. Frazer, "High-resolution time-frequency distributions for manoeuvring target detection in over-the-horizon radars," *IEE Proc.-Radar Sonar Navig.*, vol. 150, no. 4, pp. 299–304, Aug. 2003.
- [15] C. Ioana, M. G. Amin, Y. D. Zhang, and F. Ahmad, "Characterization of Doppler effects in the context of over-the-horizon radar," in *Proc. IEEE Radar Conf.*, Washington, D.C., May 2010, pp. 506–510.
- [16] C. Ioana, Y. D. Zhang, M. G. Amin, F. Ahmad, G. Frazer, and B. Himed, "Time-frequency characterization of micro-multipath signals in over-the-horizon radar," in *Proc. IEEE Radar Conf.*, Atlanta, GA, May 2012, pp. 671–675.
- [17] Y. D. Zhang, M. G. Amin, and B. Himed, "Altitude estimation of maneuvering targets in MIMO over-the-horizon radar," in *Proc. IEEE Sensor Array and Multichannel Signal Process. Workshop*, Hoboken, NJ, June 2012, pp. 257–260.
- [18] Y. D. Zhang, J. J. Zhang, M. G. Amin, and B. Himed, "Instantaneous altitude estimation of maneuvering targets in over-the-horizon radar exploiting multipath Doppler signatures," *EURASIP J. Adv. Signal Process.*, vol. 2013, no. 2013:100, pp. 1–13, May 2013.
- [19] C. Hou, Y. Wang, and J. Chen, "Estimating target heights based on the Earth curvature model and micromultipath effect in skywave OTH radar," *J. Applied Math.*, vol. 2014, article ID 424191, pp. 1–14, July 2014.
- [20] S. J. Anderson, "Target altitude estimation in OTHR via diffuse surface scatter," in *Proc. IET Int. Radar Conf.*, Hangzhou, China, April 2015, pp. 1–6.
- [21] Z. Luo, Z. He, X. Chen, and K. Lu, "Target location and height estimation via multipath signal and 2D array for sky-wave over-the-horizon radar," *IEEE Trans. Aerospace Electron. Syst.*, vol. 52, no. 2, pp. 617–631, April 2016.
- [22] H. Geng, Y. Liang, F. Yang, L. Xu, and Q. Pan, "Joint estimation of target state and ionospheric height bias in over-the-horizon radar target tracking," *IET Radar, Sonar & Navig.*, vol. 10, no. 7, pp. 1153–1167, Aug. 2016.
- [23] H. Lan, Y. Liang, Z. Wang, F. Yang, and Q. Pan, "Distributed ECM algorithm for OTHR multipath target tracking with unknown ionospheric heights," *IEEE J. Sel. Topics Signal Process.*, vol. 12, no. 1, pp. 61–75, Feb. 2018.
- [24] Y. D. Zhang and B. Himed, "Multipath Doppler difference estimation in over-the-horizon radar," in *Proc. IEEE Radar Conf.*, Oklahoma City, OK, April 2018.
- [25] J. M. Kelso, *Radio Ray Propagation in the Ionosphere*. McGraw-Hill, 1964.
- [26] K. G. Budden, *The Propagation of Radio Waves: The Theory and Radio Waves of Low Power in the Ionosphere and Magnetosphere*. Cambridge University Press, 1985.
- [27] T. J. Harris, M. A. Cervera, L. H. Pederick, and A. D. Quinn, "Separation of O/X polarization modes on oblique ionospheric soundings," *Radio Sci.*, vol. 52, pp. 1522–1533, Oct. 2017.
- [28] E. Sejdić, I. Djurović, and L. Stanković, "Fractional Fourier transform as a signal processing tool: An overview of recent developments," *Signal Process.*, vol. 91, no. 6, pp. 1351–1369, June 2011.
- [29] H. M. Ozaktas, M. A. Kutay, and Z. Zalevsky, *The Fractional Fourier Transform: With Applications in Optics and Signal Processing*. Wiley, 2001.
- [30] H-B. Sun, G-S. Liu, H. Gu, and W-M. Su, "Application of the fractional Fourier transform to moving target detection in airborne SAR," *IEEE Trans. Aerospace Electron. Syst.*, vol. 38, no. 4, pp. 1416–1424, Oct. 2002.